Dynamic Modeling of Planetary Vehicle's Fall on Soft Soil

Submitted: 23th April, 2016; accepted: 26th July 2016

Hassan Shibly

DOI: 10.14313/JAMRIS_3-2016/20

Abstract:
The objective of future planetary mission is to explore more new zones on Mars planet. This goal may be achieved by using high speed planetary vehicle, (Rover). The motion of planetary vehicles at high speed and on unknown terrain increases the number of possible risks. One risk is a sudden change of ground level in the vehicle path causes a fall down onto a low ground. This paper presents a study and simulation of the dynamic response of a free fall of a quarter vehicle (rover) model with rigid wheel on a soft soil. A simplification of Bekker's equation is derived and used in the numerical solution of the two coupled dynamic equations of motion. The Dynamic response of the unsprung mass, rigid wheel, shows a three stages; the sinkage stage, the equilibrium stage, and the pulling out stage from soil. The simulation shows that having rigid body mode helps in pulling out the vehicle wheel from the soil. It shows that the first three stages of the first fall are the most significant ones. They have the largest sinkage, largest impulsive force, and largest amplitude of the system dynamic response during interaction of the rigid wheel and the soft soil following the free fall. The existence of a damping reduces the dynamic response magnitude and prevent the unsprung mass from pulling out the wheel from soil after sinkage.

Keywords: *dynamic modeling, dynamic response, sinkage following free fall, rigid wheel soft soil mechanics*

1. Introduction

Exploration of more planetary zones requires traveling for a long distance which increases the demand for high speed planetary vehicles, rovers. High speed motion of any vehicle on unknown terrain encounters a fall dawn onto a low ground.

Planetary vehicle have metal rigid wheels to sustain the low temperatures on planets. The size of rovers and their wheels are relatively small. In addition planetary vehicles carry on instruments which are impact sensitive.

A significant part of Mars planet terrain is a loose soil which is been investigated in this work. A large number of research works were conducted on planetary vehicles traversing loose horizontal terrain for rigid wheels [1–3], for tires [4], and traversing loose sloped terrain [5]. The main focus was to investigate the traction of planetary vehicles' wheels at quasi static conditions. All previous studies did not give the necessary attention to the dynamic response of the interaction lightweight vehicles – loose terrain.

The fall of a rigid wheel on a soft soil has different mechanics than a common fall of rubber wheel on a hard ground. This case motivates the study of the mechanics during interaction rigid wheel and soft soil following rover free fall. This contribute to more understanding of the dynamic response of a rover following a free fall on a soft soil as is on Mars planet. The gained knowledge of the mechanics of the wheel-soil interaction enhances the design of future planetary vehicles.

Many studies and experiments were done to determine the mechanics of the interaction between a rigid wheel and soft soil for off road vehicles. Bekker [6] derived the analytical relationship of the normal stress σ exerted on a point on the rim of a wheel as function of the point sinkage z for sandy soil as:

$$\sigma = (k_1 + k_2 b)\left(\frac{z}{b}\right)^n \tag{1}$$

And for the shear stress τ is given by:

$$\tau(\theta) = (c_o + \sigma \cdot tan\phi)\left(1 - e^{-j/k}\right) \tag{2}$$

Where n is the wheel sinkage exponent (soil exponent), K_1 [KPa], and K_2 [KN/m^3] are pressure sinkage moduli, r is wheel radius [m], b is wheel width [m], j shear deformation distance, ϕ is internal friction angle [deg], k is the shear deformation modulus, and c_o is the soil cohesion.

Previous experiments on sand showed that the location of the maximum normal stress is a function of the slip i, where the slip is defined as one minus the ratio of actual traveling speed to the wheel linear speed. The location θ_m, see Figure 1, of the maximum normal stress on a rim of rigid wheel is given by [7] as

$$\theta_m = (c_1 + c_2 i)\theta_1 \tag{3}$$

Where c_1 and c_2 are the coefficients that define the relative location of the maximum normal stress, and θ_1 is the angular location of contact beginning, entry angle.

During rotation of the wheel each point on the contact surface of the wheel rim and the soil has sinkage z. The sinkage is determined as the difference between the vertical projections of the locations of the considered point and the first contact point. The

result is that the sinkage z is a function of the angular location θ and the wheel radius r.

The normal stress distribution, Equation (1), can be expressed as a function of the angle θ using the unique relationship between sinkage and angular location of any point on the wheel rim.

Substituting this relation into Equation (1) gives the distribution of the normal stress along the contact surface as:

$$\sigma_1(\theta) = (k_1 + k_2 b)\left(\frac{r}{b}\right)^n (cos\theta - cos\theta_1)^n \quad (4)$$

$$\sigma_2 = (k_1 + k_2 b)\left(\frac{r}{b}\right)^n \left[cos\left(\theta_1 - \frac{\theta - \theta_2}{\theta_m - \theta_2}(\theta_1 - \theta_m)\right) - cos\theta_1\right]^n \quad (5)$$

The normal stress around the wheel rim starts from zero at the free surface, at the starting point of the contact area, increases toward a maximum value, and then decreases back to zero at the end of contact with soil [7 –11]. This stress distribution is divided to two zones, 1 and 2, see Figure 1. The stress indices in the equations are referred to the zone number.

Determination of the total shear deformation distance j of a point on the wheel rim that slips in soft soil was introduced by [7, 8] as:

$$j = r[\theta_1 - \theta - (1 - i)(sin\theta_1 - sin\theta)] \quad (6)$$

Substitution of this expression into Equation (2) to obtain the shear stress new expression during slippage as:

$$\tau(\theta) = (c_o + \sigma \cdot tan\phi)\left(1 - e^{-\frac{r}{k}[\theta_1 - \theta - (1-i)(sin\theta_1 - sin\theta)]}\right) \quad (7)$$

While another approach was taken to determine the shear deformation distance j by considering the path of any point on the wheel rim as cycloid and is function of the slippage [10]. The result is more complicated expression. In this work the shear deformation distance j expression as it is in Equation (6) was adopted.

The forces that act on the contact surface of a rigid wheel during driving on a soft terrain are determined by integrating; the horizontal component of the stresses to give the horizontal force F_x, the vertical components of the stresses to give the vertical force F_z, and the shear stress on the contact area to give the torque T, as follow:

$$F_x = rb\left(\int_{\theta_2}^{\theta_1} \tau(\theta) cos\theta d\theta - \int_{\theta_2}^{\theta_1} \sigma(\theta) sin\theta d\theta\right) \quad (8)$$

$$F_z = rb\left(\int_{\theta_2}^{\theta_1} \sigma(\theta) cos\theta d\theta + \int_{\theta_2}^{\theta_1} \tau(\theta) sin\theta d\theta\right) \quad (9)$$

$$T = r^2 b \int_{\theta_2}^{\theta_1} \tau(\theta) \cdot d\theta \quad (10)$$

The nonlinearity of j expression in the shearing stress formula in equations (8)–(10) forced numerical integration in order to determine the forces and torque. In this case there is no closed form for the forces and torque that act on a wheel interacts with soft soil. The absence of closed forms prevent algebraic operation of the wheel equilibrium equations which is needed for on-line wheel-soil interaction prediction in the case of planetary missions. The on-line soil characteristics prediction requires another approach of force calculation [12].

A previous work on reformulation of the basic mechanics of a rigid driven wheel on a soft terrain was introduced by [Shibly *et al.,* 12, 13]. Recalculating the stress distribution around the rim of a driven rigid wheel that based on the experimental data given in [9] and redrawing of the stress distribution on a Cartesian Coordinates yields pattern very close to a triangle, see Figure 2. In this figure the upper three curves are the normal stress σ distribution, and the lower three curves are the shear stress τ distribution around the rim of driven rigid wheel on soft terrain for different values of soil exponent n. Therefore, the stress distribution can be approximated by triangles. A similar observation was reached by Vincent [11].

Integration of the normal stresses and sheer stresses act on the rim of a rigid wheel which interacts with soft soil is given by:

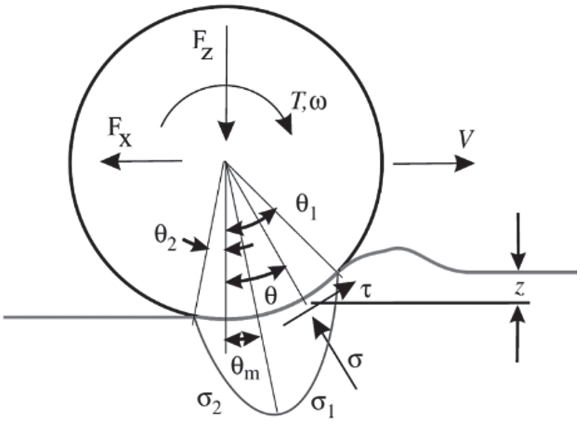

Fig. 1. Free body diagram of driven rigid wheel on soft soil [12]

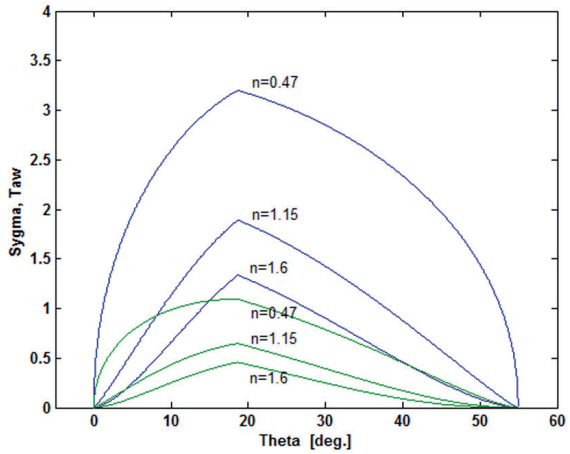

Fig. 2. Normal stress σ distribution, and shear stress τ distribution for different values of n [12]

$$F_z = rb\left(\int_{\theta_m}^{\theta_1}(\sigma_1(\theta)cos\theta + \tau_1(\theta)sin\theta)d\theta + \right.$$
$$\left. + \int_{\theta_2}^{\theta_m}(\sigma_2(\theta)cos\theta + \tau_2(\theta)sin\theta)d\theta\right) \quad (11)$$

The power of the exponent in the shear stress formula in equation (7) is nonlinear. Therefore the integration has to be done numerically. The uniqueness in the case under consideration is the accuracy of integration results and not the exact stress distribution around the rim of the wheel. The stress distribution can be approximated by an equivalent triangle, which has the same area and the same maximum stress value and θ_1 as its base. An equivalent distribution of the stresses, which act on the wheel contact surface with soft soil, was developed. Based on the equivalent stress distribution a new closed form formulation of the rigid wheel- soft soil interaction mechanics was created. A comparison between those formulations was compared with conventional formulations for forces and torque that act on the wheel. The results of the comparison shown graphically were almost matching. An experimental validation of the theoretical results was presented [12].

2. Stresses and Forces Analysis

The equivalent distribution for the two zones yields a linear stress distribution. The equivalent stress distribution S_i of normal stress σ and shear stress τ are triangles with two sides which are defined by:

$$S_i = a_i\theta + b_i\ , \quad i = 1\ right\ side, 2\ left\ side \quad (12)$$

And

$$a_1 = -\frac{S_m}{\theta_1 - \theta_m}, \quad b_1 = -a_1\theta_1$$
$$a_2 = \frac{S_m}{\theta_m + \theta_2}, \quad b_2 = a_2\theta_2 \quad (13)$$

In this work a study of the dynamic response of a rover fall down into soft soil and its penetration into a soft soil is presented. To simplify the interaction mechanics wheel-soil, and to simulate also the interaction of a round foot of a walking on soft soil a rotation less rover's wheel case was considered. The shape of the foot in this study is circular and has the same radius as of the rover's wheel. In this case the normal stress during sinkage is function of the wheel sinkage and has symmetric distribution in both sides of the vertical direction, while the maximum normal stress acts at the lowest point of the wheel as shown in Figure 3a.

In this case the equivalent distribution of the normal stresses is approximated as triangle of equal sides where $\theta_2 = -\theta_1$, $\theta_m = 0$.

Substitution of the equivalent stress distribution and integration along the wheel contact area give the normal load as:

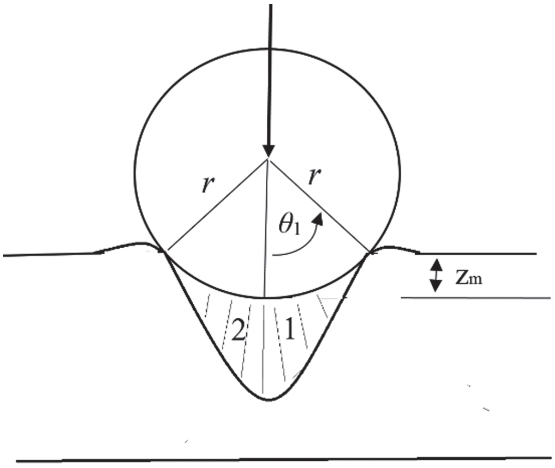

Fig. 3-a. Free body diagram of rigid wheel on soft soil

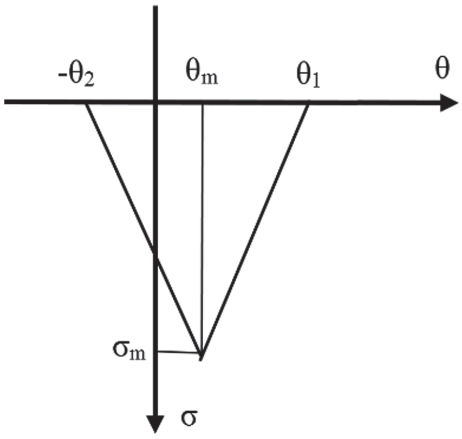

Figure 3-b. Equivalent triangle of normal stress distribution

$$F_z = 2rb\left(\int_0^{\theta_1}\sigma_1(\theta)cos\theta \cdot d\theta\right) \quad (14)$$

Substitute Equations (12 & 14) into Equation (11), and integrate to obtain the vertical force as:

$$F_z = rb\sigma_m\left(2\frac{1-cos\theta_1}{\theta_1}\right) \quad (15)$$

Plotting the expression within the parenthesis in the last equation for the range $0° < \theta_1 < 45°$ and perform a straight line fitting gives a straight line with slope of 0.98, see Figure 4. As a result the expression is simplified as it is shown in Equation (15).

$$2\frac{1-cos\theta_1}{\theta_1} \cong 0.98\theta_1 \quad (16)$$

From geometry, see Figure 3, we have:

$$1 - cos\theta_1 = \frac{z_m}{r} \quad (17)$$

Equate equation (16) and equation (17) to get a simplified relation between the entry angle θ_1 and the maximum sinkage z_m:

$$\theta_1 = \sqrt{\frac{2z_m}{r}} \tag{18}$$

Substitute into equation (15) to get:

$$F_z = rb\sigma_m\sqrt{\frac{2.0408z_m}{r}} \tag{19}$$

The maximum value of normal stress is at θ=0°. Substitute into Eq. (4) to get:

$$\sigma_m = \sigma_1(0) = (k_1 + k_2 b)\left(\frac{r}{b}\right)^n (1 - cos\theta_1)^n \tag{20}$$

After simplifications the normal force expression is:

$$F_z = (k_1 + k_2 b)\left(\frac{\sqrt{2.0408r}}{b^{n-1}}\right)(z_m)^{n+\frac{1}{2}} \tag{21}$$

The last expression of the vertical force F_z shows that the normal force is a function of the sinkage z_m during wheel sinkage into the soil. This function is nonlinear and for a specific soil parameters the coefficient of the sinkage k_z has constant value and it is defined as:

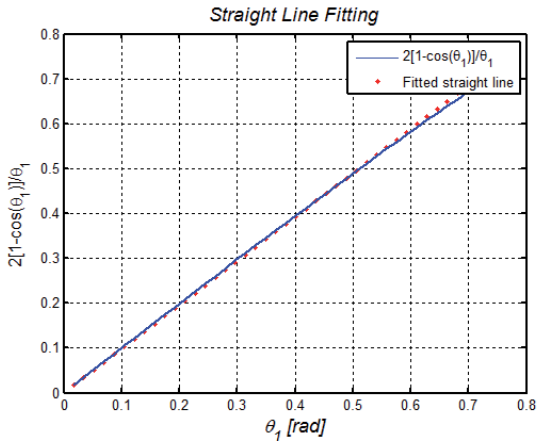

Fig. 4. Straight line fitting

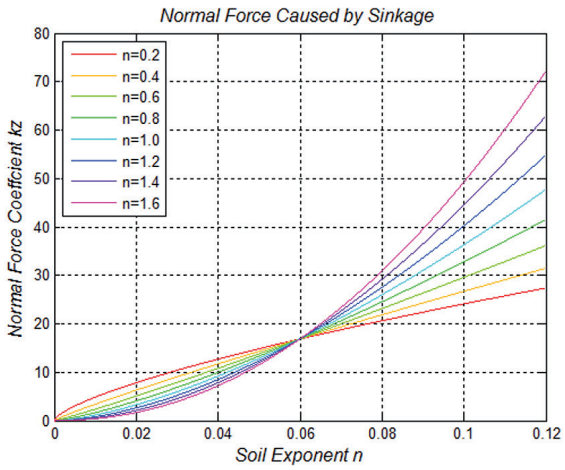

Fig. 5. Normal force of soil as function of sinkage for various values of soil exponent n

$$k_z = (k_1 + k_2 b)\left(\frac{\sqrt{2.0408r}}{b^{n-1}}\right) \tag{22}$$

And the equivalent normal force on the wheel as function of the sinkage becomes:

$$F_z = k_z(z_m)^{n+\frac{1}{2}} \tag{23}$$

A simulation of the normal force F_z as function of the sinkage z_m for various values of soil exponent n is shown in Figure 5.

To examine the increase in the coefficient value k_z as function of the soil exponent the ratio of coefficient for a two values of soil exponent n_1 and n_2 is found to be:

$$\frac{k_z(n2)}{k_z(n1)} = (b)^{n1-n2} \tag{24}$$

This ratio is computed for low and large values of soil exponent n_1=0.2, n_2=1.6, and wheel width of b=0.06[m] gives ratio of 135.5. In a similar way the ratio of the normal force F_z for a two values of soil exponent n_1 and n_2 is given by:

$$\frac{F_z(n2)}{F(n1)} = \left(\frac{z}{b}\right)^{n2-n1} \tag{25}$$

And this ratio for a sinkage value of $z=b/2$ is 0.379. This means that the soil exponent n has a significant effect on the coefficient k_z while this effect is been diminished in the formula of the normal force.

2.1. Kinematic Model

Our model of the simulation is a four wheels of rover. The rover platform is linked to the wheels by a mechanical structure. The mechanical structure's properties specify the rover stiffness and damping. In this work a simplified model of one quarter of rover is been considered. The model has two lumped masses. One is the sprung mass m_s (one quarter of rover) and it is linked to a second lumped unsprung mass m_{us}, (rigid wheel mass) by a mechanical suspension. The mechanical structure is modeled as a common linear mechanical suspension consists of linear high stiffness k_s spring and damper with low damping coefficient c_s, see Figure (6). The wheel is considered as a rigid body of radius r.

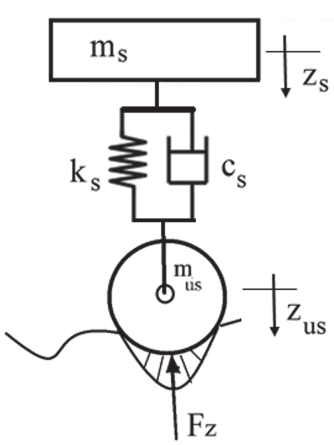

Figure 6. Dynamic model of quarter vehicle

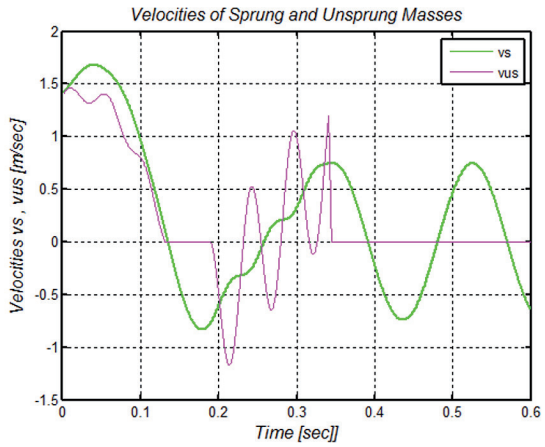

Fig. 7-a. The velocities of the sprung mass v_s and the wheel v_{us} as function of time for undamped system

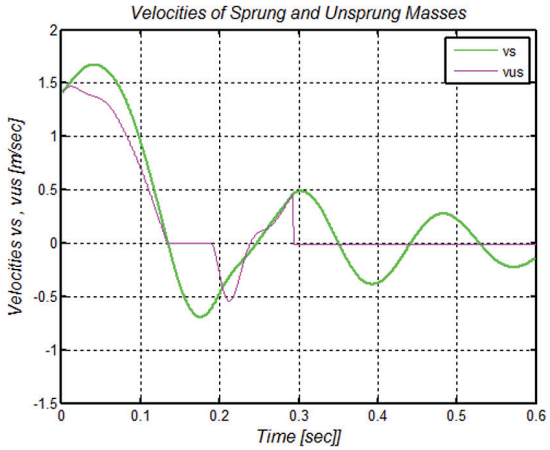

Fig. 7-b. The velocities of the sprung mass v_s and the wheel v_{us} as function of time for damped system

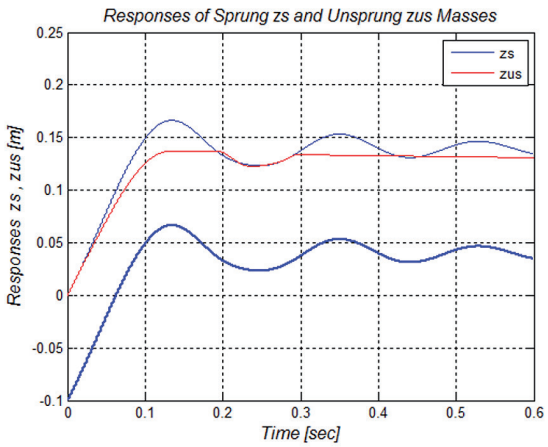

Fig. 8-a. The displacements of the sprung mass z_s and the wheel z_{us} as function of time for undamped system

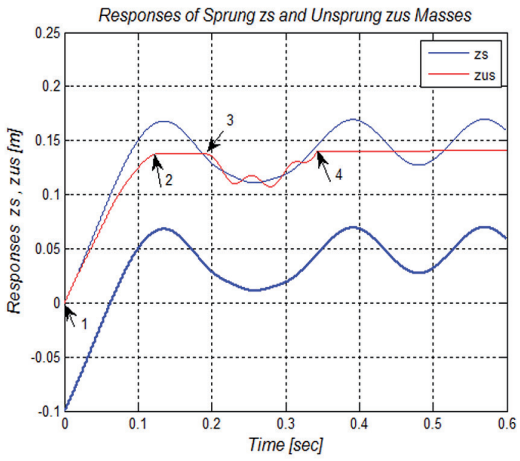

Fig. 8-b.The displacements of the sprung mass z_s and the wheel z_{us} as function of time for damped system

3. Dynamics Analysis

The dynamic response of the rover as a result of its free fall on soft soil starts at the instant of the first wheel's contact with the soil and ends when the wheel is settled down. Any bounce of the wheel leads to a second free fall and so on.

Using newton's second law for the sprung mass and for the wheel to obtain two dynamic equations of motion of the model as:

$$m_s\ddot{z}_s + c_s(\dot{z}_s - \dot{z}_{us}) + k_s(z_s - z_{us}) = m_s g \quad (26)$$

$$m_{us}\ddot{z}_{us} + c_s(\dot{z}_{us} - \dot{z}_s) + k_s(z_{us} - z_s) = m_{us}g - F_z \quad (27)$$

And in matrix form:

$$M\ddot{Z} + C\dot{Z} + KZ = F \quad (28)$$

Where:

$$M = \begin{bmatrix} m_s & 0 \\ 0 & m_{us} \end{bmatrix}, \quad C = \begin{bmatrix} c_s & -c_s \\ -c_s & c_s \end{bmatrix},$$

$$K = \begin{bmatrix} k_s & -k_s \\ -k_s & k_s \end{bmatrix}, \quad F = \begin{bmatrix} m_s g \\ m_{us}g - F_z \end{bmatrix} \quad (29)$$

The vehicle (rover) suspension structure has small damping value and we assume that it will not have a significant effect on the natural frequencies of the suspension structure and can be omitted for the purpose of determining the eigenvalues and eigenvectors [9]. As a result the following equation is used to determine eigenvalues and eigenvectors of the model:

$$det(K - \omega^2 M) = 0 \quad (30)$$

The initial conditions of the dynamic equation of motion of a quarter vehicle model are zero position and velocity equal to the final velocity of the free fall. And the external force is the interaction force between the wheel and the soft soil is the normal force F_z. Solving the last equation to obtain the eigenvalues as:

$$\lambda_1 = \omega_1^2 = 0, \ \lambda_2 = \omega_2^2 = \frac{k_s}{\mu}, \ \mu = \frac{m_s m_{us}}{m_s + m_{us}} \quad (31)$$

And the eigenvectors as:

$$\phi_1 = \begin{Bmatrix} 1.00 \\ 1.00 \end{Bmatrix}, \ \phi_2 = \begin{Bmatrix} 1.00 \\ -\eta \end{Bmatrix}, \quad (32)$$

Where μ is the reduced mass and $\eta = \frac{m_s}{m_{us}}$.

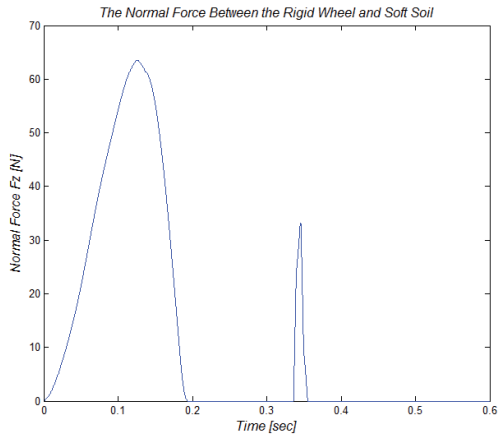

Fig. 9-a. The normal force as function of time during the two interactions for undamped system

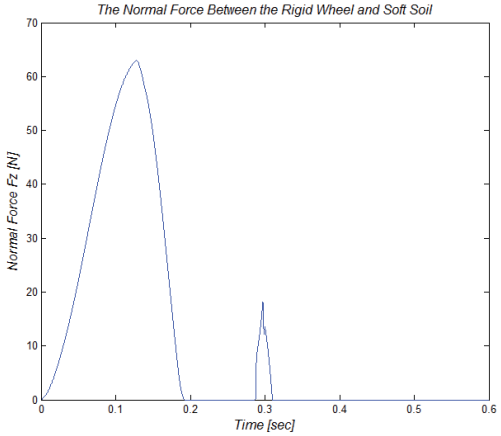

Figure 9-b. The normal force as function of time during the two interactions for damped system

The solution gives two eigenvectors (normal mode shapes). The first normal mode shape shows that the two masses move in phase as a rigid body, and the second normal mode shape shows that the two masses move out of phase with amplitude ratio of η.

The simulation results for velocity, displacement, and normal force for values of: m_s=4[kg], m_{us}=0.4[kg],r=0.12[m], g=3.7[m/sec^2], k_s=5300[N/m], c_s=25[N.sec/m] are shown in Figures 7-a&b, 8-a&b, and 9-a&b, respectively.

And in order to see the relative motion between the two masses the displacement graph z_s is shifted up by the physical dimension of the two masses (the thinner upper blue curve), see Figure 8-a & b.

5. Results and Discussion

From the simulation results we can conclude that the soil exponent *n* has a significant effect on the coefficient k_z, but this effect is significantly reduced in the magnitude of the normal force especially for the value of n=0.5. While the relative deviation from a straight line graph of the normal force F_z as function of sinkage (The straight line that passes through the origin and the graphs' intersecting point, see Figure 5) is very large. The graphs intersecting point shows that at a sinkage value equal to the wheel width the normal force has the same value for any soil exponent, which that the effect of the soil exponent *n* is cancelled.

Therefore the soil reaction during sinkage may be considered as a nonlinear spring with constant coefficient of stiffness k_z and becomes linear for n=0.5.

The interaction between the rigid wheel (unsprung mass) and soft soil has three stages. At each stage the normal force F_z is different. During the first stage the wheel penetrates into the soft soil until it reaches its maximum sinkage at zero velocity, it is between point 1 & point 2 on the graph, see Figure 8-a. At this stage the normal force is been calculated according to the expression in Equation (23). The second stage starts at maximum sinkage and ends at the instant of pulling out leaving the soil, and it is between point 2 & point 3 on Figure 8-a. The wheel velocity at stage two is zero and the normal force is the reaction force to all other forces which act on the wheel. The third stage starts when the sprung mass pulls out the unsprung mass (wheel) and then the wheel losses contact with the soil, it is between point 3 & point 4 on Figure 8-a. During the third stage the normal force is zero and the system starts to vibrate according to its two eigenvectors with an initial conditions equal to the motion parameters at the end of the second stage.

It can be noticed that there is a significant effect of the rigid body mode at the start of stage three. This mode is useful in pulling out the wheel from the soil.

At the first stage the penetration is linearly increases with time as shown in Figure 8, and the penetration speed into the soil is affected by the normal projection of soil stresses on the wheel's rim, and the transmitted forces caused by the sprung mass. The transmitted forces act on the wheel toward down in the direction of the wheel's motion.

The first fall makes the soil more compact, as a result the soil parameters are changed. Therefore it is harder to penetrate into the soil and then it harder to pull out compared to the first fall. In case that the wheel does not pull out leads to a continuous vibration of the sprung mass about its final position.

Adding damping to the system reduces the vibration of both sprung mass, and unsprung mass (wheel) significantly. Also the maximum value of the force in the second sinkage is much less than the first one. The damper is very essential if the fall occurs on earth as it is expected, but in space it is preferred not to have damper and let the sprung masses vibrates which may help in pulling out the wheel from the soil.

The normal force during sinkage and contact with soil exists during very short time and it has a geometric shape resemblance to any impulsive force during collision of two objects. Therefore a future work is to replace the sinkage force with an impulsive force applied to the wheel during contact with a soft soil.

AUTHOR

Hassan Shibly – Central Connecticut State University, New-Britain, CT, 06050, USA.
E-mail: hshibly@ccsu.edu

REFERENCES

[1] Ding L., Deng Z., Gao H., Nagatani K., Yoshida K., "Planetary rovers' wheel-soil interaction mechanics, new challenges and applications for wheeled mobile robots", *Journal of Intelligent Service Robotics*, vol. 4, 2011, no. 1, 17–38. DOI: 10.1007/s11370-010-0080-5.

[2] Azimi A., Holz D., Kovecses J., Angeles J., Teichmann M., *Efficient Dynamics Modeling for Rover Simulation on Soft Terrain*, AIAA, 2012, 0804.

[3] Irani R. A., Bauer R. J., Warkentin A., "Dynamic Wheel-Soil Model for Lightweight Mobile Robots with Smooth Wheels", *Journal of Intelligent & Robotic Systems*, vol. 71, 2013.

[4] Taheri S., Sandu C., Taheri S., Pinto E., Gorsich D., "A technical survey on Terramechanics models for tire–terrain interaction used in modeling and simulation of wheeled vehicles", *Journal of Terramechanics*, vol. 57, 2015, 1–22.

[5] Li Z., Wang Y., "Coordinated Control of Slip Ratio for Wheeled Mobile Robots Climbing Loose Sloped Terrain", *Scientific World Journal*, 2014. DOI: 10.1155/2014/396382.

[6] Bekker M.G., *Theory of Land Locomotion, the Mechanics of Vehicle Mobility*, University of Michigan Press Ann Arbor, 1956.

[7] Wong J.-Y., Reece A.R., "Prediction of Rigid Wheel Performance of Driven Rigid Wheels, Part I", *Journal of Terramechanics*, vol. 4, no. 1, 1967, 81–98.

[8] Onafko O., A. R. Reece., "Soil Stresses and Deformation Beneath Rigid Wheels", *Journal of Terramechanics*, vol. 4, no. 1, 1967, 59–80.

[9] Wong Jo. Y., *Theory of Ground Vehicles*, John-Willey & Sons, New-York, 2001.

[10] Janosi Z., "An Analyses of Pneumatic Tire Performance on Deformable Soils". In: *Proc. First Int. Con. On Terrain Vehicle Systems*, Edizon Minerva Tecnica, Torino, 1961.

[11] Vincent E.T., "Pressure distribution on and Flow of Sand Past Rigid Wheel". In: Proc. First Int. Con. On Terrain Vehicle Systems, Edizon Minerva Tecnica, Torino, 1961, 859–877.

[12] Shibly H., Iagnemma K., Dubowsky S., "An equivalent soil mechanics formulation for rigid wheels in deformable terrain, with application to planetary exploration rovers", *Journal of Terramechanics*, vol. 42, 2005, 1–13.

[13] Iagnemma K., Shibly H., Rzepniewski A., Dubowsky S., "Planning and control algorithms to enhance rover rough terrain mobility". In: *Proceeding of I-SAIRAS: 6th International Symposium on Artificial Intelligence, Robotics, and Automation in Space*, USA, June 2001.

[14] Clough R.W., Penzien J., *Dynamics of Structures*, McGraw Hill, 1975.